Jordan Journal of Physics

ARTICLE

Morphological Characterization of Eutectic Si and Ge Phases in the Corresponding Al-15Si and Al-20Ge Alloys Using FIB Tomography

N. Wanderka[a], **H. Kropf** [a] and **M. Timpel** [b]

[a] *Helmholtz Zentrum Berlin für Materialien und Energie GmbH, Hahn-Meitner Platz 1. 14109 Berlin, Germany.*

[b] *Department of Industrial Engineering, University of Trento, via Sommarive 9, 38123 Trento, Italy.*

Abstract: The three-dimensional morphology of the eutectic Ge phase in samples modified by Ca and Y in the hypoeutectic Al-20Ge alloy has been investigated by focused ion beam tomography. Addition of Ca (0.2 wt.%) caused a modification of the eutectic Ge phase from a branched plate-like morphology to a compressed cylinder-like shape of smaller dimensions. Addition of Y (0.2 wt.%) resulted in a transformation of the eutectic Ge phase with two types of morphology. One type is vermicular-like in 2D and refined plate-like in 3D, while the other appears as a holey Ge matrix with an embedded eutectic Al phase of rod-like morphology. The morphology of the modified eutectic Ge has been discussed in terms of possible growth mechanisms compared with that of the as-cast non-modified Al-20Ge alloy and that of well-known Sr-modified eutectic Si in Al-Si system.

Keywords: Hypoeutectic Al-Ge alloys, Modification of eutectic Ge phase, Focused ion beam tomography, Scanning electron microscopy.

Introduction

Aluminium-silicon eutectic alloys are important industrial foundry materials. Small additions of sodium [1] or strontium produce a spectacular change of the eutectic silicon microstructure. The refinement or modification of the eutectic silicon from a uniform lamellar (plate-like) structure to fibrous structure is accompanied by a great improvement of mechanical properties, like tensile strength, elongation and hardness of the alloy. The modification effect in Al-Si alloys has been the subject of numerous studies for decades and a large number of theories was proposed to understand the modification phenomena [2-7]. With the development of a new analytical method, namely laser-assisted atom probe tomography (APT) that allows the examination of element distributions on the atomic scale, Timpel et al. [8, 9] and Barrirero et al. [10],

investigated the modification of Al-Si alloys by Sr addition. These studies showed that unlike previous beliefs, it was not the single modifying atom, i.e., Sr, but Al-Si-Sr co-segregations that are responsible for modification of the eutectic Si phase in the Al-Si system. Timpel et al. [8, 9] demonstrated that such co-segregations are absorbed at the "twin-plane re-entrant edges" (TPRE growth mechanism) on the internal eutectic Al/Si interface and prevent further growth in the current direction, thus the Si crystal changes its growth to energetically favored directions.

Modification of the eutectic Si phase from lamellar plate-like to a fine fibrous structure has also been obtained by additions of Ba, Ca and Eu [7, 11-13], even though the level of modification is different from one case to another. The strongest modifier among them has been found

Corresponding Author: Nelia Wanderka   **Email:** wanderka@helmholtz-berlin.de

to be Sr. In the past, modifiers were selected mainly in such a way that the atomic radius of the modifier only slightly differs from that of Si. Addition of modifiers like Y and Yb to the Al-7Si alloy was found to only refine the eutectic Si [11].

Comparable to the binary Al-Si eutectic alloy, Ge and Al form the similar simple eutectic binary Al-Ge system. According to their phase diagrams, the eutectic point in Al-Si is at 12.7 wt.% Si (eutectic temperature at 577 °C) and in Al-Ge at 53 wt.% Ge (at 424 °C) [14]. Both Si and Ge have a diamond crystal structure; therefore, it may be expected that the modification phenomenon is similar in both binary eutectic systems. Unlike Al-Si alloys, which have been extensively studied, the Al-Ge system has rarely been investigated [2, 15]. Hellawell [2] reported on the growth and structure of eutectics with Si and Ge based on observations mainly by optical microscopy. Li et al. [15] recently reported on the effect of trace elements Ca and Y on the eutectic Ge phase in an Al-20Ge alloy. A detailed microstructure characterization was performed on the nanometer scale using high-resolution transmission electron microscopy (HRTEM) and APT. However, a morphological characterization of the complex irregular shapes of the modified eutectic Ge phase in two dimensions (2D) using optical microscopy, scanning electron microscopy (SEM) or TEM is difficult. This information in three dimensions (3D) from the nanometer to micrometer range is missing. The nano-sectioning method using focused ion beam (FIB), which is able to produce 3D tomograms from 2D SEM images as described by Lasagni et al. [16], was successfully applied for visualization of Fe-rich phases, their location within the eutectic Al-Si grains [17,18] or of as-cast and modified structures of an Al-12Si alloy [19].

The objective of the present work is therefore the study of the morphological changes of the eutectic Ge phase by additions of Ca and Y to draw conclusions of the possible growth mechanisms based on the observations using FIB tomography. The results obtained for the Al-Ge system have been compared with those of an Al-15Si alloy modified by Sr. In addition, the microstructure has been characterized by SEM images of the sample surface.

Experimental

Two types of alloy with nominal composition Al-20Ge and Al-15Si (composition in wt.%) were prepared using arc melting. The Al-20Ge alloy was prepared from high-purity Al and Ge (99.998% purity) at Montanuniversität Leoben, Austria. Additions of 0.2Y (wt.%) and 0.2Ca (wt.%) with purity of 99.8% (both Y and Ca) were added to the Al-20Ge alloy. The Al-15Si (wt.%) alloy was cast at the Faculty of Metallurgical and Materials Engineering of the Indian Institute of Technology Madras, Chennai, India. The alloy components were of commercial purity. More details about sample preparation and composition of Al-15Si alloy can be found in Ref. [17]. The Al-15Si alloy was modified by 62 ppm Sr. The cooling rate of the Al-20Ge alloy was ~3.3 K/sec and that of the Al-15Si alloy ~6.5 K/sec.

All samples for SEM investigations have undergone standard metallographic preparation procedures like mechanical polishing, grinding and finally polishing with a colloidal silica suspension. A Zeiss 1540 EsB CrossBeam® workstation, which combines a FIB column with a SEM column, was employed for the microstructure characterization. The imaging of the sample surface was performed with a low acceleration voltage of 2-5 kV using the InLens® secondary electron (SE) detector. The use of the low acceleration voltage allows to obtain high-resolution images [20]. The Zeiss 1540 EsB CrossBeam® workstation was also employed for 3D visualization of the eutectic Ge and the eutectic Si using FIB-energy-selective backscattered (FIB-EsB) tomography by serial sectioning and imaging as described in Refs. [17, 21]. Slices of about 25 nm (50 nm) thickness for Al-20Ge (Al-15Si) were cut out of the sample by a 30 keV Ga ion beam at an ion current of 500 pA, resulting in an constant voxel size of $25 \times 25 \times 25$ nm³ ($50 \times 50 \times 50$ nm³). The in-column EsB electron detector was used for imaging the 2D slices with an acceleration voltage of 2 kV and a grid voltage of -1.5 kV. Since the EsB detector allows the detection of elastically backscattered (high-angle) electrons with a high-resolution signal at the nanometer scale, the eutectic microstructure of the alloys was well resolved and sufficient imaging contrast was obtained. The 3D reconstruction of the investigated volumes was performed using the software VG Studio MAX 2.0.

Results

Microstructure of the Alloys Investigated by SEM

The microstructure of the investigated Al-20Ge, Al-20Ge-0.2Ca and Al-20Ge-0.2Y alloys is demonstrated in Figs. 1a, b and c, d, respectively. The Al-20Ge alloy (Fig. 1a) consists of primary α-Al dendrites, as well as eutectic Al and Ge phases. The eutectic Ge phase imaged by SE InLens® detector can be distinguished by the light grey contrast, whereas primary α-Al dendrites and eutectic Al phase are imaged in dark grey. The eutectic Ge phase shows a branched network consisting of lamellae and corrugated crystals. The microstructure of the Al-20Ge-0.2Ca and Al-20Ge-0.2Y alloys differs from that of the Al-20Ge alloy by a finer eutectic Ge phase in the presence of Ca and Y and a clear change in the morphology of the crystals, as can be seen in Figs. 1b, c and d. Furthermore, apart from the α-Al dendrites and the eutectic Al and Ge phases that form in the binary system, intermetallic phases with lengths of several tens of μm were also found. The intermetallic phases are well discernable because of their rod- or needle-like morphology in 2D. In the corresponding alloys, they are of Al_2Ge_2Ca (not shown here) and Al_2Ge_2Y type.
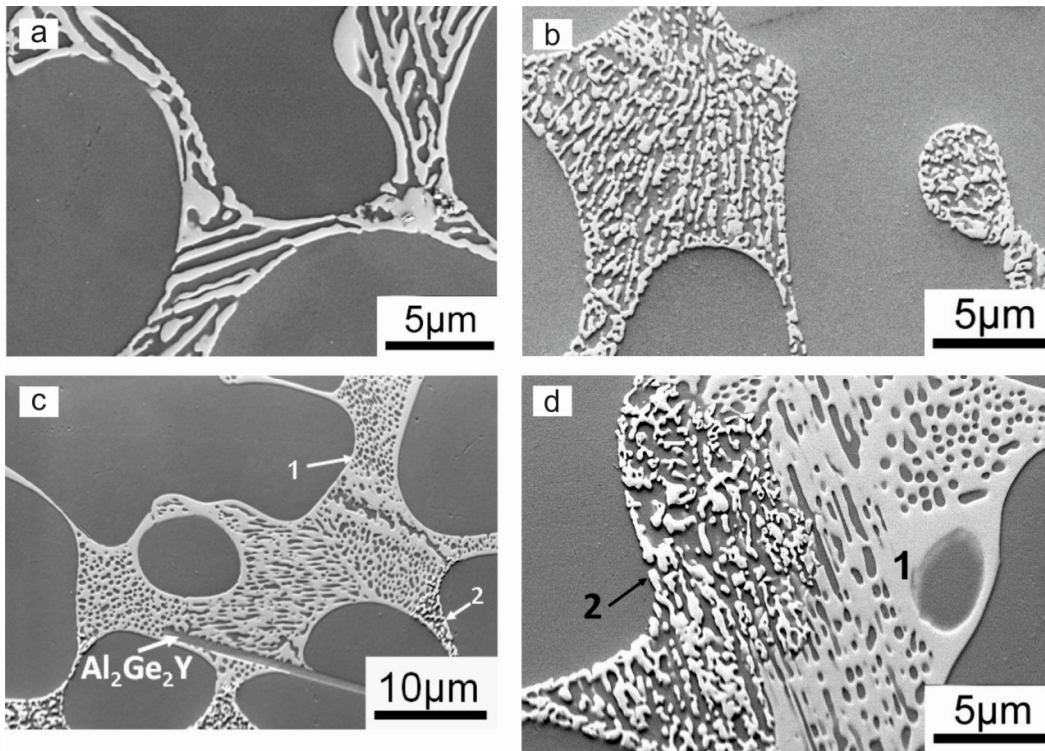

FIG. 1. Microstructure of a) Al-20Ge, b) Al-20Ge-0.2Ca and c) Al-20Ge-0.2Y alloys visualized by the InLens® SE detector; d) enlarged view of the eutectic microstructure of the Al-20Ge-0.2Y alloy.

The morphology of the eutectic Ge phase in Figs. 1b and c, d (region marked by 2 in Figs. 1c and d) is similar. However, Ca additions produced a quite uniform eutectic Ge phase (Fig. 1b) regarding size and morphology, while in the alloy with Y additions (Figs. 1c and d), there are two regions (marked by 1 and 2) with different structures. Region 1 indicates a holey Ge matrix with an embedded eutectic Al phase of rod-like morphology, while the structure of the region 2 appears as small eutectic Ge precipitates of irregular shape. The eutectic Ge phase in region 1 is slightly darker in contrast than in region 2. The eutectic Al phase inside region 1 looks like small rods with diameters ranging from 0.25 to 0.38 μm and their length axis lies between 1.26 and 5.85 μm. A typical intermetallic Al_2Ge_2Y phase with rod-like morphology is shown in Fig. 1c.

The typical microstructure of the unmodified and the Sr-modified Al-15Si alloy is illustrated in Fig. 2a, b and 2c, d, respectively. It is noteworthy that for the comparison of their

7

microstructure (i.e., compare Fig. 2a, c and 2 b, d, respectively) the magnification of the SEM images has been adapted to the size of the corresponding microstructure. The eutectic Si phase (bright contrast) exhibits coarse plates in the unmodified alloy (Fig. 2a, b), while in the Sr-modified alloy (Fig. 2c, d) it appears as a much finer and mixed structure of thin Si platelets and fibrous Si. The difference in the magnification emphasizes the modification effect (i.e., higher magnification needed for the Sr-modified Al-Si microstructure).
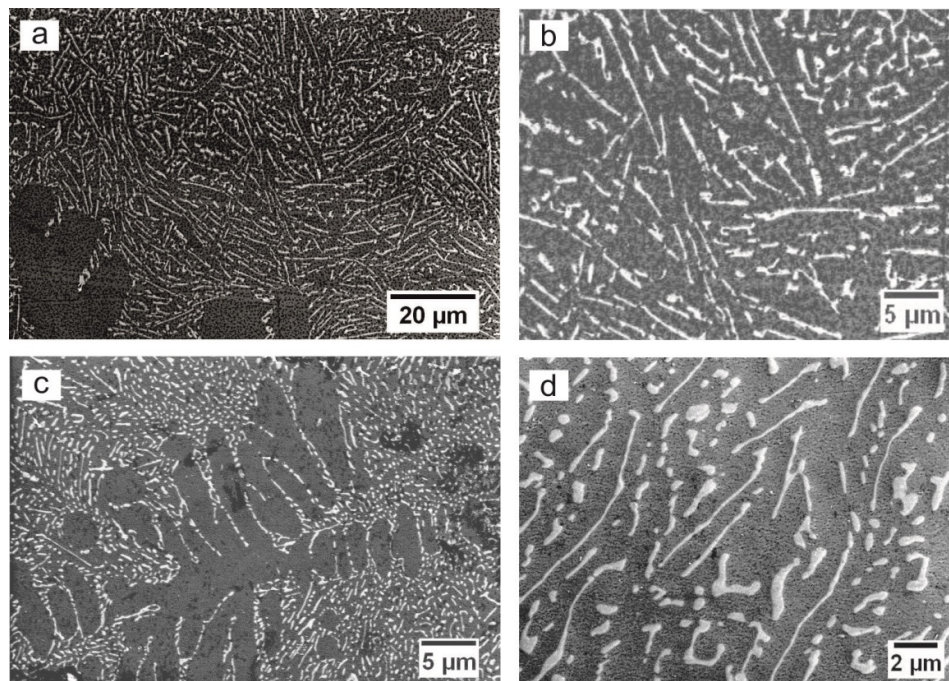

FIG. 2. Microstructure of a,b) unmodified and c,d) Sr-modified Al-Si alloy visualized by the InLens® SE detector. Note the difference in the magnification of the SEM images.

FIB Tomography

Al-20Ge-based Alloys

Figs. 3, 4 and 5 show the Al-Ge eutectic microstructure of the Al-20Ge, Al-20Ge-0.2Y and Al-20Ge-0.2Ca alloys in 3D by means of FIB-EsB tomography. In the unmodified Al-20Ge alloy, the eutectic Ge (in cyan) and eutectic Al phase (in blue) are illustrated in Fig. 3a within an analyzed volume of $11 \times 6 \times 4$ μm³. The primary α-Al phase is marked by A. A separate visualization of the 3D morphology of the eutectic Ge phase is shown in Fig. 3b. It should be noted that the dimension in z direction is reduced from 4 to 1.56 μm in order to better visualize the real size and shape of the eutectic Ge phase. The lamella-like eutectic Ge phase in 2D observed by SEM (Fig. 1a) consists of plates in 3D as can be seen after the FIB tomography shown in Fig. 3b. The 3D image clearly indicates that the eutectic Ge phase grows in a branched manner, thus forming an interconnected Ge network. The average thickness of the coarse branched Ge plates in the xy-imaging plane was measured to be 0.84 μm and the length axis can reach sizes larger than 10 μm.

Fig. 4a shows the 3D microstructure of Al-20Ge-0.2Ca alloy in an analyzed volume of $11 \times 6 \times 4.7$ μm³. For the sake of clarity, only a part ($11 \times 0.6 \times 3.8$ μm³) of the entire volume is shown in Fig. 4b and a magnified part is illustrated in Fig. 4c. As can be seen from Fig. 4b and c, the eutectic Ge phase is much finer than in the unmodified alloy. Its morphology appears as compressed cylinder-like structures that have an elliptical cross-section. The average width of the ellipses is ~ 0.35 μm and their length is about 1.65 μm. The height of the compressed cylinders is difficult to measure, but it is roughly bigger than the length of the cylinder axis truncated by the analyzed volume. The compressed cylinders are often connected with each other, forming a network.
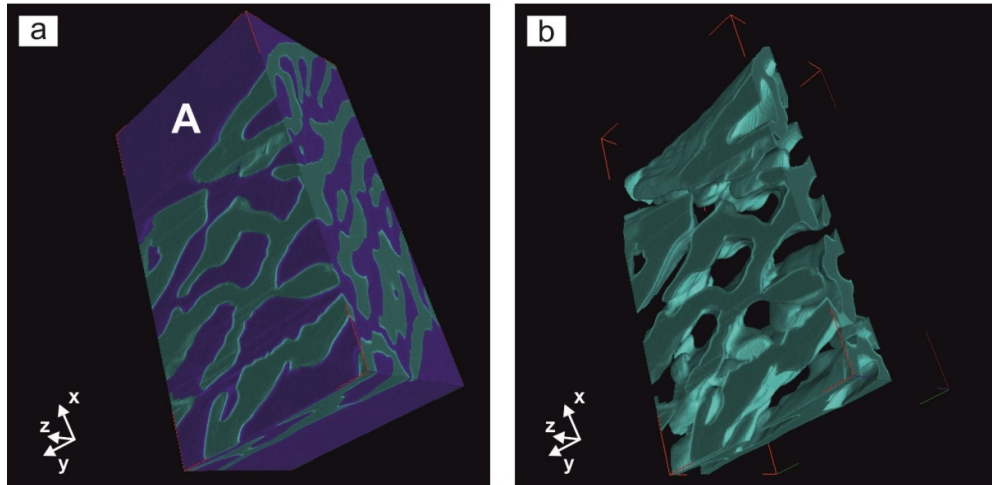
FIG. 3. a) 3D morphology of the eutectic Ge phase (cyan) embedded in the eutectic Al phase (blue) in an investigated volume of $11 \times 6 \times 4$ µm³ of unmodified Al-20Ge alloy; primary α-Al phase is marked by A; b) the eutectic Ge phase is presented in a reduced volume of $11 \times 6 \times 1.56$ µm³.
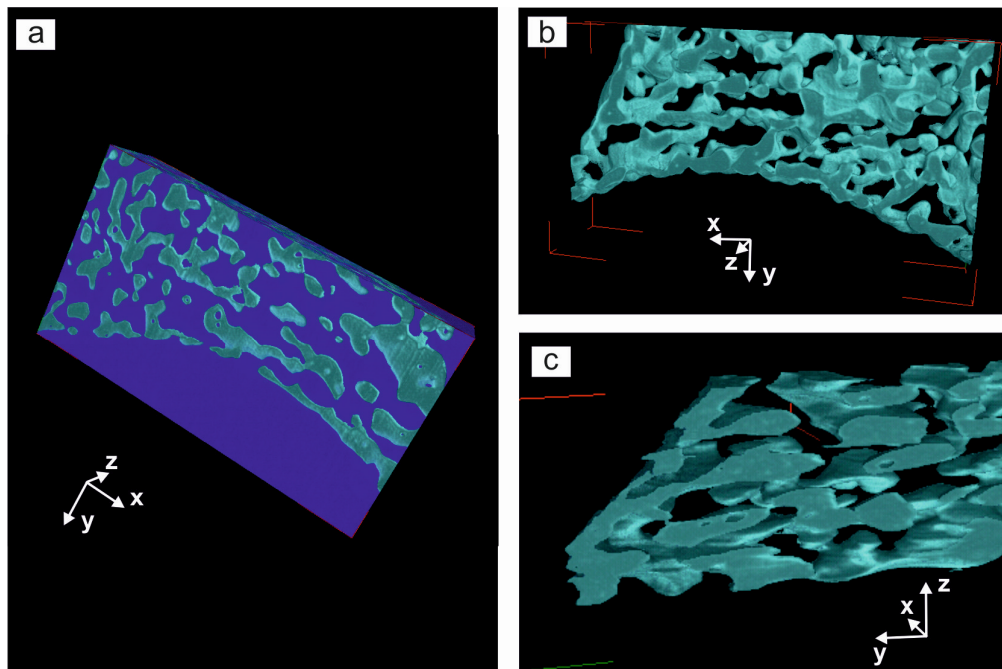

FIG. 4. a) 3D morphology of the eutectic Ge phase (cyan) embedded in the eutectic Al phase (blue) in an investigated volume of $11 \times 6 \times 4.7$ µm³ of the Al-20Ge-0.2Ca alloy; b) the eutectic Ge phase is presented in a reduced volume of $11 \times 0.6 \times 3.8$ µm³; c) enlarged view of a part of the eutectic Ge phase with compressed cylinder-like morphology shown in b).

For the Al-20Ge-0.2Y alloy, Fig. 5a demonstrates the 3D microstructure in an investigated volume of $11 \times 6 \times 4$ µm³. The microstructure consists of the eutectic Ge and Al phases and primary α-Al phase which is marked by A. Two different morphologies of the eutectic Ge phase were observed, marked by 1 and 2, which is in agreement with the SEM observations of the sample surface (Fig. 1c and d). These two different morphologies of the eutectic Ge phase can be more clearly seen from the thin volume section (thickness ~ 0.16 µm), as shown separately in Fig. 5b and c for the eutectic Ge and Al phase, respectively. The eutectic Ge phase in region 1 has a higher volume fraction than that in region 2. The 3D morphology of the

9

eutectic Ge phase in region 1 does not appear as plates, but as a holey eutectic Ge matrix (Fig. 5b, see higher magnification in Fig. 5c), in which the eutectic Al phase with a rod-like morphology (Fig. 5d, region 1) is embedded. The diameter of the rod-like eutectic Al phase as measured from 3D images is about 0.4 ± 0.05 μm (where the error corresponds to the 2σ deviation). The value

lies in the range of the typical diameter measured from the SEM image in Fig. 1c (i.e., 0.25-0.38 μm). In contrast, the eutectic Ge phase in region 2 exhibits a complex structure with highly curved surfaces and a vermicular-like shape as can be seen in the thin slice of the investigated volume. The diameter of the vermicular-shaped eutectic Ge phase is about 0.2 μm.

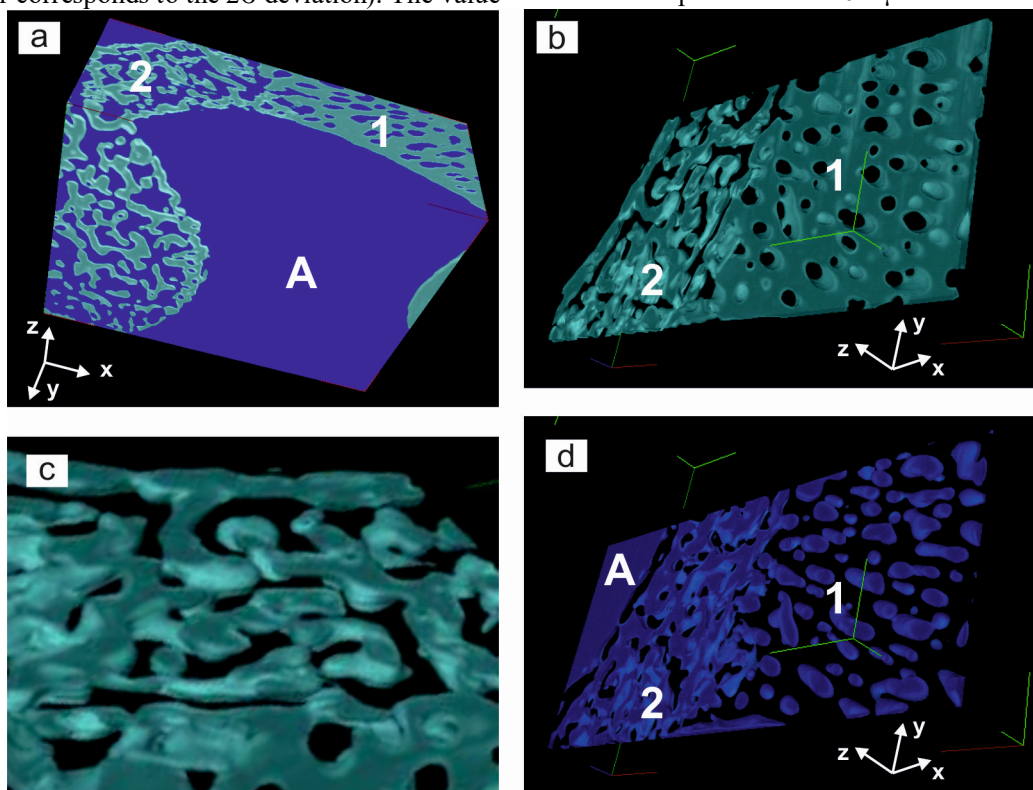
FIG. 5. 3D morphology of the eutectic Ge phase (cyan) embedded in the eutectic Al phase (blue) in an investigated volume of $11 \times 6 \times 4$ μm³ of the Al-20Ge-0.2Y alloy: a) two regions with different morphologies of the eutectic Ge phase are marked by 1 and 2; primary α-Al is marked by A; b) eutectic Ge; c) higher magnification of region 2 and d) eutectic Al phases are presented in a reduced volume of $11 \times 6 \times 0.16$ μm³.

Al-15Si-based Alloys

Fig. 6 displays the morphology of the 3D eutectic Al-Si microstructure of the unmodified (Fig. 6a,b) and Sr-modified (Fig. 6c,d) Al-15Si alloy. The unmodified Si phase with plate-like morphology is illustrated in Fig. 6b and the Sr-modified Si phase is shown in Fig. 6c. The eutectic Si plates are very thin with a thickness between 0.2 μm and 0.5 μm. They are truncated by the surface of the analyzed volume and therefore, their total length could be much larger

than visualized by the data set. The Sr-modified eutectic Si phase shows a partially modified structure (Fig. 6d), which is in agreement with the corresponding SEM images of the sample surface (Fig. 2c and d) and previous observations of the alloy using FIB-EsB tomography [17]. The diameter of the eutectic Si fibers is in the range between 0.3 μm and 0.7 μm, whereas the thin Si platelets are much smaller and thinner than the Si plates in the unmodified Al-15Si alloy.
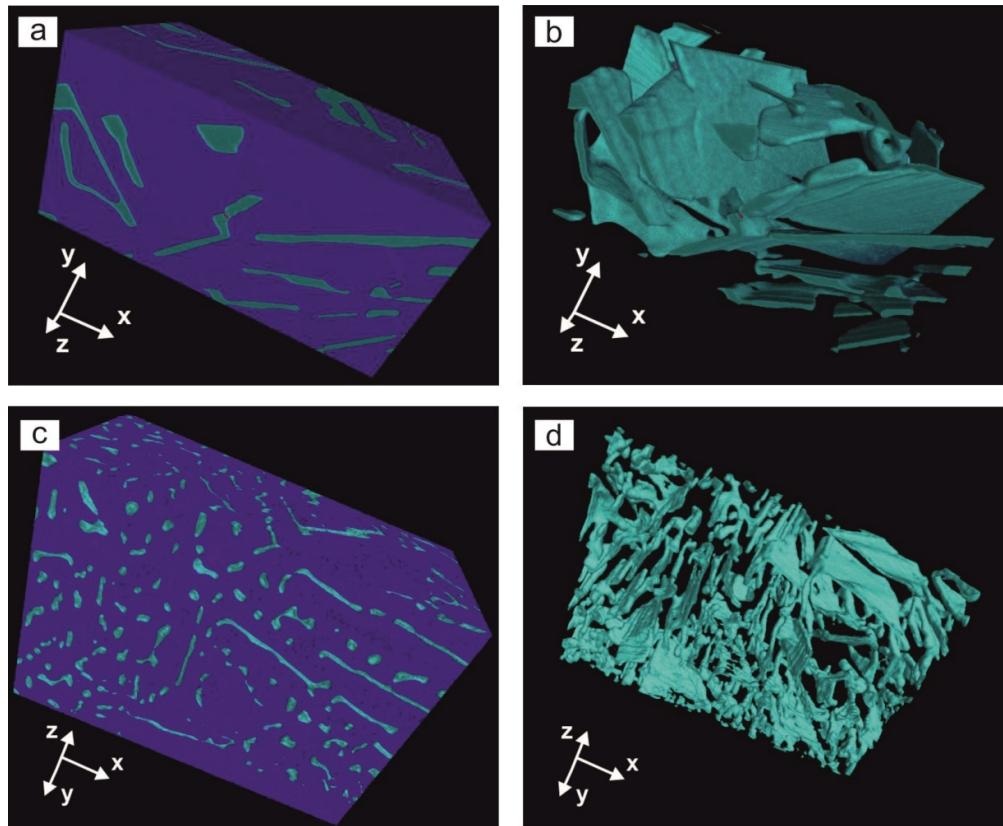
FIG. 6. a) 3D morphology of the eutectic Si phase (cyan) embedded in the eutectic Al phase (blue) in an investigated volume of $20 \times 10 \times 13$ µm³ of the unmodified Al-15Si alloy; b) unmodified eutectic Si phase only; c) 3D morphology of the eutectic Si phase (cyan) embedded in the eutectic Al phase (blue) in an investigated volume of $27 \times 19 \times 12$ µm³ of the Sr-modified Al-15Si alloy; d) Sr-modified eutectic Si phase only.

Discussion

Unmodified Al-Si and Al-Ge Alloys

Both the Al-Si- and the Al-Ge-based alloys mainly comprise the irregular binary eutectic microstructure, which is the type of eutectic that can be typically found in metal/non-metal systems. The eutectic Al phase is non-faceted, while the eutectic Si-/Ge- phase is faceted. In such systems, the eutectic develops an irregular structure, as the growth of the Si and Ge crystals is strongly anisotropic along the close-packed {111} planes of the diamond cubic structure, resembling large plates as can be seen from the FIB tomography shown in Figs. 3a, b and 6a, b. The plate-like phases have a significant kinetic barrier to grow in certain directions as is the case in particular for the eutectic Si phase. Branching of Si and Ge crystals or termination of growth occurs, i.e., no constant lamellar spacing exists during growth of irregular eutectics. According to Fisher and Kurz [22], the faceted Si and Ge plates lead ahead of the eutectic Al matrix, since they have the smallest constitutional undercooling, and the non-faceted eutectic Al phase follows. In contrast to the regular eutectic, where the two phases grow with a similar growth rate, the irregular eutectic Al and Si/Ge phases grow with different growth rates. However, coupled growth is always maintained. As soon as the eutectic Si/Ge phase begins to grow, Al is rejected at the solidification front and *vice versa*, Si or Ge atoms are rejected on the solidification front of the eutectic Al phase. This alternating sequence of solute rejection leads to a non-isothermal growth interface, which locally provides conditions for simultaneous growth of both eutectic phases. This growth mechanism has also been observed during *in-situ* solidification of an Al-10Si-0.3Fe alloy during X-ray synchrotron tomography experiments [23].

11

However, besides the similarities of the two systems, there are also differences in the microstructure as seen in Figs. 3a, b and 6a, b. The unmodified Al-Ge alloy exhibits a much larger volume fraction of eutectic Ge (36.5 vol.% [2]) compared to the eutectic Si (13.6 vol.% [17]) phase in the unmodified Al-Si alloy. Consequently, the eutectic Ge plates are much coarser than the eutectic Si plates when comparing the width of the plates seen in Fig. 3a and 6a, respectively. The overall morphology and formation of the 3D network of the eutectic Ge and Si plates (compare Figs. 3b and 6b) are also different. The cause lies in the different growth mechanism of Si and Ge. The eutectic Si crystal grows mainly as individual faceted plates with {100} faces. The eutectic Ge crystal, besides faceted crystals, shows also corrugated crystals with alternating {111} faces. The formation of corrugated crystals can be explained by the fact that Ge forms growth twins much easier and there is no preferential growth texture in <100> direction as in Si. Otherwise, Hellawell [2] argued the complex regular growth forms of the eutectic Ge phase as a consequence of the more symmetrical form of the Al-Ge phase diagram [14].

Modification by Sr, Ca and Y

Al-15Si Alloy Modified by Sr

The phenomenon of modification of the eutectic Si phase by Na [1], Sr [7-10, 24, 25], Ba, Ca, Y and Yb [11] has been widely studied. Many mechanisms of growth and nucleation of the eutectic Si phase were proposed for modification, but only a few mechanisms were established and are commonly accepted, such as "poisoning of TPREs" [4, 26] and "impurity-induced twinning" (IIT) [7]. According to Nogita et al. [11], among Ba, Ca, Y and Yb, the best modification of the eutectic Si phase has been obtained by addition of Ba. Addition of Ca produced also a very fine Si fibrous structure. Y and Yb only refined the eutectic Si phase, but it remains plate-like. It is noteworthy that the twin density in the eutectic Si phase was found to be similar for all the modified samples, even though Ba and Ca showed strong modification, whereas Y and Yb only refined the eutectic Si phase. The conclusion is that the IIT mechanism does not strongly influence the change of the eutectic Si growth direction. In fact, the recently gained knowledge at the atomic scale using APT [8, 9] evidences is that within the eutectic Si phase (in

an Al-10Si-based commercial alloy), nanometer sized rod-like Si-Al-Sr co-segregations, which form at the solidification front, restrict the growth direction. The plate-shaped branched networks shown in Fig. 6a, b finally change into a branched coral network of fibers (Fig. 6c, d) by adding the modifying element Sr. In the Sr-modified Al-15Si alloy, a mixed morphology (i.e., thin platelets and fibrous structure) of the eutectic Si phase is visible (Fig. 6c, d). The lower Sr content (62 ppm) in this alloy results in an only partially modified morphology of the eutectic Si phase during eutectic solidification, whereas a well-modified structure of the eutectic Si phase can be achieved at Sr levels in the range of 80 - 120 ppm (depending on the alloy purity and cooling rate) [25].

Al-20Ge Modified by Ca

The sufficient amount of the eutectic modifiers Ca and Y to produce a significant change in the morphology of the eutectic Ge phase has not been determined so far, but the effect of Ca and Y on an Al-7Si-based (A356.0) alloy has been investigated by Nogita et al. [11]. The maximum modification of the eutectic Si phase (transition from flakes to fibers) was achieved by 210 ppm Ca, while Y additions in the range between 700 and 5200 ppm cause only a refinement of the Si plates. The present results for the Al-Ge system reveal a refined eutectic Ge phase by additions of both Ca and Y. However, a large excess of Ca and Y (0.2 wt.% in the present study) produces also µm-sized intermetallic compounds of the type Al_2Ge_2Ca (not shown here, but they are present in the alloy with Ca additions) and Al_2Ge_2Y, which are typical characteristics of an over-modified alloy. This result is in agreement with observations by Hellawell [2]. Ludwig et al. [12] reported that Al_2Si_2Ca intermetallic phases occur already at 39 ppm (300 ppm) Ca addition to an Al-7Si commercial purity (high-purity) alloy. An increased level of Sr (500 ppm) to an Al-7Si alloy produced also large Sr-containing intermetallic phases. However, Dahle et al. [25] suggested that in addition to the formation of Sr-containing intermetallic phases, the high amount of Sr was rather correlated with the reversion of eutectic nucleation. It appears that the formation of intermetallic compounds depends on many factors, such as modifier type and content, metalloid type and the purity of the alloy.

In the Al-Ge alloy with Ca addition, the size and morphology of the eutectic Ge phase change from coarse branched Ge plates (unmodified alloy) to compressed cylinder-like morphology of smaller dimensions, being connected and building a network. The formation of the network can be explained based on the impingement of individual Ge particles during their growth. According to their morphology, the growth of individual Ge particles occurs in two preferential directions (one is the main axis of the compressed cylinder and the other one is the longer axis of the elliptical cross-section). The crystals of the modified eutectic Ge phase are coarser but shorter than the crystals of the modified eutectic Si phase. In contrast, Ca produces Si fibers in Al-Si alloys [11] with only one preferential growth direction, i.e., along the fibers. As mentioned above, studies on the Al-Ge system are rather rare [2, 15], but there is a significant amount of research on the Al-Si system. However, since Si and Ge crystals exhibit the same diamond structure, we assume that their behavior with respect to modification is similar. In the Al-Si system, the addition of the modifier usually causes a decrease of the eutectic temperature and a shift of the eutectic point to higher Si concentrations. An increase in the recalescence undercooling and a decrease of the eutectic temperature by Sr addition to an Al-10Si alloy have also been reported by McDonald et al. [24]. Ludwig et al. [12] showed that 50 ppm Ca addition to Al-7Si (A356 commercial purity alloy) refined the eutectic Si phase, but coarsened it in the high-purity alloy [12], whereas Ca additions higher than 300 ppm do not change the morphology of the eutectic Si phase [12]. Ludwig et al. [12] suggested that Ca suppresses the nucleation and growth and thereby alters the morphology of the eutectic Si phase. The morphology transition of the eutectic Ge phase in the present work could be then explained by the larger kinetic undercooling with Ca addition. The growth rate of the modified eutectic Ge phase should be lower than that of the unmodified one, indicating that the overgrowth by the eutectic Al matrix occurs more frequently and the crystal shape will become more complex. The density of twins in both the unmodified and the Ca-modified eutectic Ge phase has been observed to be very low [15], which indicates that the IIT mechanism plays no significant role in the modification of the eutectic Ge phase. Although the number of twins greatly increases in Sr-modified Al-Si alloys, Timpel et al. [8, 9] and Barrirero et al. [10] came to the same conclusion that the IIT mechanism does not significantly affect the growth direction of the eutectic Si phase. As mentioned above, the rod-like Al-Si-Sr co-segregations restrict the growth direction of the eutectic Si phase. In the case of the eutectic Ge phase in the Al-20Ge system, Li et al. [15] reported on the presence of rod-like Al-Ge-Ca co-segregations with a diameter of ~ 3 nm and a length of ~ 58 nm as measured by APT. Their total length could be longer, because they were truncated on one side of the surface of the analyzed APT volume. They contain Al (32.02 ± 2.78) at.%, Ge (58.28 ± 2.18) at.%, Ca (5.98 ± 3.27) at.% and O (3.72 ± 3.13) at.%. We assume that such types of co-precipitates induced the morphological change of the Ge crystals similar to that of Si in Al-Si alloys [8-10]. However, more detailed investigations are required to clarify whether the high amount of Ca (2000 ppm) as modifier or the Ge itself is responsible for the formation of the compressed cylinder-like morphology instead of fibers.

Al-20Ge Refined by Y

As shown in Figs. 1c, d and Fig. 5, the microstructure of Al-20Ge with Y addition differs from that with Ca addition. Moreover, there are two regions (1 and 2) in the eutectic Ge phase, which clearly depict different morphologies. It should be mentioned that the volume fraction of Ge in region 1 is much larger than that in region 2 (see Fig. 1c). The holey eutectic Ge phase (Fig. 5b) of region 1 contains a rod-like eutectic Al phase (Fig. 5d). The colonies of the eutectic Al rods are all oriented more or less in the same direction within a single eutectic Ge grain. The explanation for the obtained microstructure in region 1 can be as follows: the eutectic reaction starts with the formation of the Ge crystals nucleating at the Al dendrites and Ge builds a continuous phase front around Al dendrites. Ge grows forward and the Al solute is rejected at the solid-liquid front, leading to the formation of Al clusters. Such clusters segregate and grow to rod-like structures. During further solidification, the Ge crystals tend to overgrow the eutectic Al rods due to their higher growth rate. This growth process is continuously repeated and at the end of solidification, it creates the microstructure of region 1 presented in Figs. 1c, d and 5b. Regarding the orientation

13

of the eutectic Al rods within a eutectic Ge grain, it can be concluded that the eutectic Al rods strongly depend on the orientation of the eutectic Ge phase and grow epitaxially on a {111} plane in the <110> direction. Columnar eutectic Al phase with a strong texture in <110 > direction has also been observed in a Sr-modified Al-Si alloy [6]. The composition of these eutectic Al rods could not be measured yet. However, APT measurements [15] showed much smaller Y-enriched particles embedded in the eutectic Ge phase. The composition of the Y particles was measured to be $Al_{69}Ge_9Y_{22}$, which is close to the stable equilibrium phase Al_3Y, assuming that Al is partially substituted by Ge. Li et al. [15] reported on another type of particles containing Y with the composition $Al_{42}Ge_{49}Y_5O_4$. This composition, however, does not correspond to the stable Al_2Ge_2Y intermetallic phase that was observed by SEM (see Fig. 1c). A tendency to form nanometer sized Al-rich (14 at.% Al) clusters within the eutectic Ge phase of the as-cast Al-Ge alloy has been already reported by Li et al. [15]. Although the maximum solubility of Al in Ge according to the binary Al-Ge phase diagram is less than 2 at. % at 400°C [14], the eutectic Ge phase in the as-cast alloy showed a significantly high concentration of Al (5.4 at.%) [15].

Region 2 shows an irregularly shaped eutectic Ge phase. At the first glance, the morphology of the Y-modified eutectic Ge phase looks similar to that modified with Ca. However, a closer inspection of the FIB tomograms reveals that region 2 looks like a miniature of the unmodified eutectic Ge phase illustrated in Fig. 3b. Indeed, the thickness (0.2 μm) of the eutectic Ge phase with Y additions is four times smaller than that of the unmodified alloy (0.84 μm), but the morphology is still the same. The microstructure of region 2 indicates a significant decrease in the size of the eutectic Ge phase, i.e., a refinement. Our observations are in good agreement with the results presented by Nogita et al. [11], where only plate-like refinement by Y in an Al-7Si alloy has been found. Refinement of the eutectic Si phase is known to be obtained in high-purity hypoeutectic Al-Si alloys without Sr additions [24, 27] when compared to that of commercial purity alloys.

Our conclusion concerning the role of Y addition to an Al-20Ge alloy is that it creates a constitutionally undercooled zone thus increasing the number of nuclei, which refines the microstructure.

Summary

Morphological changes of the eutectic Ge phase by addition of the modifiers Ca and Y to an Al-20Ge alloy and of the eutectic Si phase by addition of the modifier Sr to an Al-15Si alloy have been investigated using FIB tomography. There are a number of similar, but also different, features in the two eutectic binary alloys:

- Both alloys in the unmodified state show a plate-like morphology of the eutectic Si/Ge phases. The eutectic Si grows as individual (but interconnected) plates and the eutectic Ge as a highly branched network of coarse plates. This is a result of the preferential growth in one direction of the eutectic Si phase, whereas the eutectic Ge phase can grow without any preferential direction. The eutectic Si plates are much thinner than the eutectic Ge plates, which is due to the higher volume fraction of the eutectic Ge phase in Al-Ge-based alloys.
- The addition of Sr and Ca modifies the eutectic Si and Ge phase, respectively. However, the addition of Sr changes the morphology of the eutectic Si phase from plate-like to fine fibers, whereas the addition of Ca changes the morphology of the eutectic Ge phase from branched plates to compressed cylinder-like shapes. The difference in the morphologies of the two modified eutectic microstructures can be ascribed to the different growth behaviors of the Si and Ge crystals.
- Addition of Y to the Al-20Ge alloy only results in a refinement of the eutectic Ge phase. Two types of refinement region can be obtained. The morphology of the eutectic Ge phase in one region is similar to that of the unmodified alloy, but four times smaller. The eutectic Ge phase in the second region represents a holey eutectic Ge phase with an embedded rod-like eutectic Al matrix.

Acknowledgments

References

[1] Pacz, A., Alloy, U.S. Patent No. 1387900 (1921).

[2] Hellawell, A., Prog. Mater. Sci., 15 (1970) 3.

[3] Hanna, M.D., Lu, S.-Z. and Hellawell, A., Metall. Trans. A., 15 (1984) 459.

[4] Kobayashi, K.F. and Hogan, L.M., J. Mater. Sci., 20 (1985) 1961.

[5] Shamsuzzoha, M. and Hogan, L.M., J. Cryst. Growth, 76 (1986) 429.

[6] Shamsuzzoha, M. and Hogan, L.M., Philos. Mag. A, 54 (1986) 459.

[7] Lu S.Z. and Hellawell, A., Metal. Mater. Trans. A, 18 (1987) 1721.

[8] Timpel, M., Wanderka, N., Schlesiger, R., Yamamoto, T., Lazarev, N., Isheim, D., Schmitz, G., Matsumura, S. and Banhart, J., Acta Mater., 60 (2012) 3920.

[9] Timpel, M., Wanderka, N., Schlesiger, R., Yamamoto, T., Isheim, D., Schmitz, G., Matsumura, S. and Banhart, J., Ultramicroscopy, 132 (2013) 216.

[10] Barrirero, J., Engstler, M., Ghafoor, N., de Jonge, N., Odén, M. and Mücklich, F., J. Alloys Compd., 611 (2014) 410.

[11] Nogita, K., Drennan, J. and Dahle, A.K., Mater. Trans., 44 (2003) 625.

[12] Ludwig, T.H., Schaffer, P. and Arnberg, L., Metal. Mater. Trans. A, 44 (2013) 3783.

[13] Li, J., Hage, F., Wiessner, M., Romaner, L., Scheiber, D., Sartory, B., Ramasse, Q. and Schumacher, P., Sci. Rep., 5 (2015) 13802.

[14] Hansen, M. and Anderko, K., "Constitution of binary alloys", (McGraw-Hill Publ. Co., Inc., New York/Toronto/London, 1958).

[15] Li, J.H., Wanderka, N., Balogh, Z., Stender, P., Kropf, H., Albu, M., Tsunekawa, Y., Hofer, F., Schmitz, G. and Schumacher, P., Acta Mater., 111 (2016) 85.

[16] Lasagni, F., Lasagni, A., Holzapfel, C., Mücklich, F. and Degischer, H.P., Adv. Eng. Mater., 8 (2006) 719.

[17] Timpel, M., Wanderka, N., Murty, B.S. and Banhart, J., Acta Mater., 58 (2010) 6600.

[18] Timpel, M., Wanderka, N., Grothausmann, R. and Banhart, J., J. Alloys Compd., 558 (2013) 18.

[19] Lasagni, F., Lasagni, A., Marks, E., Holzapfel, C., Mücklich, F. and Degischer, H.P., Acta Mater., 55 (2007) 3875.

[20] Reimer, L., "Scanning electron microscopy: physics of image formation and microanalysis", (Springer, Berlin, 1998).

[21] Uchic, M.D., Holzer, L., Inkson, B.J., Principe, E.L. and Munroe, P., MRS Bulletin 32 (2007) 408.

[22] Fisher, D.J. and Kurz, W., Acta Metall., 28 (1980) 777.

[23] Yu, J.M., Wanderka, N., Rack, A., Daudin, R., Boller, E., Markötter, H., Manzoni, A., Vogel, F., Arlt, T., Manke, I. and Banhart, J., Acta Mater., 129 (2017) 194.

[24] McDonald, S.D., Nogita, K. and Dahle, A.K., Acta Mater., 52 (2004) 4273.

[25] Dahle, A.K., Nogita, K., Zindel, J.W., McDonald, S.D. and Hogan, L.M., Metal. Mater. Trans. A, 32 (2001) 949.

[26] Day, M.G. and Hellawell, A., Proc. Roy. Soc. A, 305 (1968) 473.

[27] Yu, J.M. Wanderka, N., Miehe, G. and Banhart, J., Intermetallics, 72 (2016) 53.